Journal of Saudi Chemical Society (2019) **23**, 284–293

King Saud University

Journal of Saudi Chemical Society

www.ksu.edu.sa
www.sciencedirect.com

ORIGINAL ARTICLE

Physicochemical characteristic of neodymium oxide-based catalyst for *in-situ* CO_2/H_2 methanation reaction

Salmiah Jamal Mat Rosid [a,*], **Susilawati Toemen** [b], **Wan Azelee Wan Abu Bakar** [b], **A.H. Zamani** [c], **Wan Nur Aini Wan Mokhtar** [d]

[a] *Unisza Science and Medicine Foundation Centre, Universiti Sultan Zainal Abidin, Kampus Gong Badak, 21300 Kuala Nerus, Terengganu, Malaysia*
[b] *Department of Chemistry, Faculty of Science, Universiti Teknologi Malaysia, 81310 UTM Skudai, Johor, Malaysia*
[c] *Faculty of Industrial Sciences & Technology, Universiti Malaysia Pahang, 26300 Gambang, Kuantan, Pahang, Malaysia*
[d] *School of Chemical Sciences and Food Technology, Faculty of Science & Technology, Universiti Kebangsaan Malaysia, 43600 Bangi, Selangor, Malaysia*

Received 25 June 2018; revised 2 August 2018; accepted 3 August 2018
Available online 16 August 2018

KEYWORDS

Neodymium oxide;
Methanation;
Carbon dioxide;
Natural gas;
Greenhouse gases

Abstract Carbon dioxide emission to the atmosphere is worsened as all the industries emit greenhouse gases (GHGs) to the atmosphere, particularly from refinery industries. The catalytic chemical conversion through methanation reaction is the most promising technology to convert this harmful CO_2 gas to wealth CH_4 gas for the combustion. Thus, supported neodymium oxide based catalyst doped with manganese and ruthenium was prepared via wet impregnation route. The screening was initiated with a series of Nd/Al_2O_3 catalysts calcined at 400 °C followed by optimization with respect to calcination temperatures, based ratios loading and various Ru loading. The Ru/Mn/Nd (5:20:75)/Al_2O_3 calcined at 1000 °C was the potential catalyst, attaining a complete CO_2 conversion and forming 40% of CH_4 at 400 °C reaction temperature. XRD results revealed an amorphous phase with the occurrence of active species of RuO_2, MnO_2, and Nd_2O_3, and the mass ratio of Mn was the highest among other active species as confirmed by EDX. The ESR resulted in the paramagnetic of Nd^{3+} at the g value of 2.348. Meanwhile nitrogen adsorption (NA) analysis showed the Type IV isotherm which exhibited the mesoporous structure with H3 hysteresis of slit shape pores.

* Corresponding author.
E-mail address: salmiahjamal@unisza.edu.my (S.J.M. Rosid).
Peer review under responsibility of King Saud University.

ELSEVIER Production and hosting by Elsevier

1. Introduction

Today's natural gas is one of the fastest components of energy consumption in the world. The requirement energy was constantly for household activities, electricity and transportation [1,2]. For Malaysia, natural gas is the future energy and these

https://doi.org/10.1016/j.jscs.2018.08.002
1319-6103

are ensured by large reserves of Malaysia and higher strength with large gas reserves in the neighboring countries [3]. In 2001, the country exported 49.7% of natural gas liquefied natural gas (LNG) to Japan, South Korea and Taiwan under long-term contracts [4]. However, the presence acid gas of carbon dioxide in natural gas will not only corrode the pipeline, lower the quality of natural gas and reduce the value of natural gas in the market but also can be harmful to the environment. When burning, untreated natural gas will release CO_2 gas, which is considered as the main greenhouse gas in the environment [5]. The release of the greenhouse gases affects the climate changes and human health. Therefore, it is necessary to develop a technology that will enable us to use fossil fuels while reducing emissions of greenhouse gases. Among other techniques, membrane technology is selected as the most practical technology. However, these methods are not effective if it involves high content of CO_2 gas and low selectivity toward toxic gas separation. The high cost that needed at all stage of providing customers with natural gas will be a burden to our government [6]. Because of these issues, catalytic methanation reaction has been designed and proposed due to its effectiveness to simultaneously convert CO_2 to CH_4 gas, assisted with heterogeneous catalyst [7–9]. In the purge of natural gas, carbon dioxide conversion to methane is an important process whereby hydrogen gas is used together with carbon dioxide gas through the methanation process as shown in Eq. (1) below [10].

$$CO_2 + 4H_2 \xrightarrow{\text{catalyst}} CH_4 + 2H_2\ O \quad (1)$$

The important requirement for selecting the correct catalyst system lies in its ability to receive and activate CO_2. Moreover, the acidic properties of CO_2 require the use of catalyst system with the Lewis basic properties. These requirements are apparently suitable with some transition metal oxides and lanthanide oxides. Their acid and redox properties can be improved by adding other oxides [11,12]. The investigation was conducted by Wang et al. [13] who found that the CO_2 adsorption strength was controlled by the Lewis base of the catalyst, the center of the metal surface d-band, and charge transfer from the metal surface to the chemisorbed CO_2 [14]. The conventional nickel based catalyst has been widely used before due to low cost however, this catalyst will give higher CO_2 conversion only at high reaction temperature and also sensitive toward chemical attack by forming cokes. Therefore, recently among catalysts used, lanthanide oxide has been widely employed as a based in methanation reaction such as cerium, lanthanum, samarium, and praseodymium. Recently, researchers have successfully studied the potential of cerium as an oxygen storage vacancy in which higher CO_2 conversion (97.73%) and 91.31% CH_4 formation were achieved using Ru/Mn/Ce (5:30:65)/Al_2O_3 catalyst in flue gases [15] whereas Ru/Mn/Ce (5:35:60)/Al_2O_3 performed 100% CO_2 conversion and 80% CH_4 formation for CO_2 methanation in simulated natural gas [16]. Other than cerium, samarium also has been utilized as a based catalyst in CO_2 methanation reaction with 100% CO_2 conversion and 93.46% CH_4 formation under molar ratio of 4:1 (H_2:CO_2) [17]. Similarly, the CO_2 conversion and CH_4 formation were also investigated using praseodymium and lanthanum oxides as a based in methanation reaction with 100% CO_2 conversion and 41% CH_4 formation [8,18]. The potential lanthanum as a promoter also has been further investigated by Wierzbicki et al. [19] and they concluded that medium strength of basic site in rare earth metal has affected the CO_2 adsorption capacity by improving the reducibility of active species and weakening the interaction between metal. The optimum loading of La was considered as an important aspect that affect the reducibility and increase the basicity of the catalyst in methanation reaction [20].

Previously, neodymium is one of lanthanide oxide which provides a good performance in electrical and optical properties [21,22]. Long and Wan [23] have investigated the activity of neodymium oxide doped with strontium fluoride for oxidative coupling of methane. It was found that the addition of Nd_2O_3 into SrF_2 lattice has increased the basicity, conductivity and dispersion of surface active sites. However, the methane conversion was increased from 26.6% to 33.7% at 700 °C with GHSV = 20,000 h^{-1}. In addition, neodymium also has been used as a dopant in methanation [24] in which the addition of small amount of neodymium has stabilized the nickel oxide against degradation of its textural properties and gave a complete CO_2 conversion at 350 °C. Nevertheless, up to the present time, there was no literature reporting on the use of neodymium oxide as a based catalyst in methanation reaction. The CO_2 conversion using cobalt doped with ruthenium was also studied by Zhu et al. [25]. The performance of cobalt doped with ruthenium showed that the selectivity of CH_4 was higher (>90%) at 200 °C as compared to monometallic cobalt catalyst which only gave 50% CH_4 selectivity at 300 °C. This study showed that the addition of Ru to cobalt oxide has enhanced the performance of the respective catalyst. Therefore, the present study focuses on the synthesis, physicochemical properties and catalytic activity of neodymium doped manganese with ruthenium as co-dopant and evaluation of its promoting effect toward CO_2 methanation reaction.

2. Experimental

2.1. Synthesis of $Ru/Mn/Nd/Al_2O_3$

The supported Ru/Mn/Nd (5:20:75)/Al_2O_3 catalysts with various calcination temperatures were synthesized by means of incipient wetness impregnation technique using manganese nitrate, $MnNO_3$ as the dopant and ruthenium (III) chloride hydrate, $RuCl_3{\cdot}H_2O$ as co-dopant. In a typical synthesis, neodymium (III) nitrate hexahydrate (5.00 g) was dissolved in 4 mL distilled water and mixed with a 2.29 g of $MnNO_3$ and 0.23 g $RuCl_3$ with 10 mL of distilled water. Next, 3 mm of alumina beads with surface area , 253 m^2/g was immersed in the mixed solution for 24 h. Then, the supported catalysts were dried in the oven at 80–90 °C for 24 h and followed by calcination in the furnace under atmosphere at 400 °C, 700 °C, 800 °C, 900 °C, 1000 °C, and 1100 °C for 5 h at a flow rate of 10 °C/min. Table 1 shows the composition of each amount of based, dopant and co-dopant at various temperatures.

2.2. Catalytic testing

The catalytic testing of CO_2 methanation was performed in a house-built microreactor (tube length of 300 mm and tube size of 25 mm ID) equipped with Fourier Transform Infrared Nicolet Avatar 370 DTGS and operated at atmospheric pressure. The analysis was carried out using simulated natural

Table 1 Composition of synthesis neodymium oxide based catalyst at various ratios and temperatures.

Catalysts	Ratio, %	Calcination temperature, °C
Nd	100	400
Mn/Nd	40/60	400
Mn/Nd	30/70	400
Mn/Nd	20/80	400
Mn/Nd	10/90	400
Ru/Mn/Nd	5/35/60	1000
Ru/Mn/Nd	5/30/65	1000
Ru/Mn/Nd	5/25/70	1000
Ru/Mn/Nd	5/20/75	400, 700, 800, 900, 1000, 1100
Ru/Mn/Nd	5/15/80	1000
Ru/Mn/Nd	10/15/75	1000
Ru/Mn/Nd	15/10/75	1000

gas with a composition of 20% for CO_2 and 80% for H_2 with ratio (1:4) and flow rate of 50 mL/min in an isothermal tube furnace. Each trial was tested on a new catalyst sample for the purpose of preventing any ambiguous results due to loss of activity or any changes that might occur during reactions that cannot be retained by regeneration. Prior to the catalytic testing, catalysts are first subjected to air pruning at 100 °C for 30 min in order to activate the catalysts. After cooling process at room temperature, the reactant gas was introduced into the microreactor system without catalyst as a calibration. Thereafter, the reactant gas was passed through the catalyst and the temperature was elevated to the desired reaction temperatures. The product stream was collected in FTIR sample cells with KBr windows embedded and scanned using FTIR Nicolet Avatar 370 DTGS spectrophotometer. FTIR spectra were recorded in the range of 4000–450 cm^{-1} at 5 scan resolutions to ensure better signal to noise ratio. The GHSV was kept fixed at 636 mL $g^{-1}h^{-1}$ and methane formation is determined by Hewlett-Packard 6890 Series GC System (Ultra 1) with nominal column. Helium gas was used as a carrier gas with a flow rate of 20 mL/min at 75 kPa, and using Flame Ionization Detector (FID) with the injection port temperature at 150 °C, detection temperature at 310 °C and oven temperature at 40 °C. The catalyst was first preheated at 100 °C for 1 h to remove the moisture and hence activate the catalyst. The measurements were done at reaction temperatures of 100 °C, 200 °C, 300 °C and 400 °C. The percentage of CO_2 conversion calculation is shown in Eq. (2) [26].

$$\%\ \text{of}\ CO_2\ \text{Conversion} = \frac{\text{Peak Area of}\ CO_2\ \text{calibration} - \text{Peak Area of}\ CO_2\ \text{conversion}}{\text{Peak area of}\ CO_2\ \text{calibration}} \times\ 100\% \quad (2)$$

Meanwhile, the methane formation and selectivity to methane are calculated using Eqs. (3) and (4) below:

$$\%\ \text{Selectivity to}\ CH_4 = \frac{[CH_4]\ \text{from GC}}{[\text{Converted}\ CO_2]\ \text{from FTIR}} \times\ 100\% \quad (3)$$

$$\%\ \text{Yield of}\ CH_4 = \frac{[CH_4]\ \text{from GC}}{\%\ \text{Conversion of}\ CO_2} \times\ 100\% \quad (4)$$

2.3. Characterization of catalysts

X-ray diffraction (XRD) was analyzed using Diffractometer D5000 Siemens Crystalloflex with Cu K_α radiation (λ = 1.54060 Å) at a scanning range of 2θ range 10°–80°. Field emission scanning electron microscopy (FESEM) images were obtained on a Zeiss Supra 35 VP with energy of 15.0 kV coupled with EDX analyzer. Samples were blasted using an electron gun with a tungsten filament under 25 kV resolution to obtain the required magnification image. The BET surface area was determined by nitrogen adsorption/desorption at −196 °C using Micromeritics ASAP 2010. The samples were degassed at 120 °C for 5 h and left under vacuum to cool down at ambient temperature before analysis. The electrons spin resonance (ESR) spectrometer was conducted by inserting sample powder into a 4 mm × 0.5 mm quartz tube using Thermo-Flex3500 model. ESR measurements are carried out in the temperature range between 4.5 K and 300 K using a 100 kHz modulation frequency and a 2 G configuration amplitude. The microwave capacity can be reduced in the range between 200 mW and 0.2 μW and was adjusted in such a way so that it does not have any saturation effect. The reducibility and CO_2 desorption of the catalyst was performed by temperature programmed reduction (TPR) and CO_2-temperature programmed desorption (CO_2-TPD) using Micromeritics Autochem 2920. The TPR analysis was conducted by heating the catalyst up to 1000 °C under 10% H_2 in a quartz U-tube (internal diameter = 10 mm) and cleaned under Ar flow of 20 mL/min at 150 °C for 2 h. The CO_2-TPD was completed by placing an appropriate amount of catalyst sample in a quartz U-tube (internal diameter = 10 mm) and was cleaned under He flow for 20 mL/min at 150 °C for 1 h. The TGA-DTA curves were obtained by TGA-SDTA 851 Mettler Toledo simultaneous thermal analyzer.

3. Results and discussion

3.1. Catalytic activity measurement using FTIR analysis

The activities of a series of alumina supported neodymium oxide based catalysts for the CO_2 conversion are displayed in Fig. 1. From the screening, the bimetallic oxide of Mn/Nd (30:70)/Al_2O_3 catalyst exhibited the highest CO_2 conversion with 38% as compared to monometallic oxide catalysts. The higher loading of 70 wt% of Nd immersed in the catalyst would enhance the activity of hydrogenation to produce methane as the increasing amount of active surface site in the supported catalyst [27]. However, excessive loading of

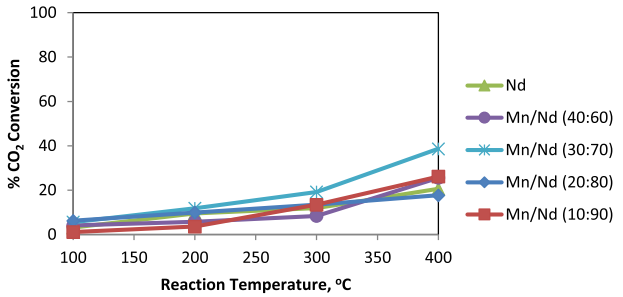

Fig. 1 CO_2 conversion over various ratios of Mn/Nd catalyst supported with Al_2O_3 calcined at 400 °C for 5 h.

Nd deteriorates the catalytic activity, decreasing in CO_2 conversion which might due to blockage of the active site.

Therefore, the inferior performance of supported bimetallic oxide catalysts has encouraged the study of trimetallic oxide. The addition of Ru as co-dopant improved the catalytic activity on CO_2 conversion as the presence of Ru favors the reduction process and dispersion on the surface of the catalyst. Overall, the CO_2 conversion obtained for Ru/Mn/Nd (5:40:55)/Al_2O_3, Ru/Mn/Nd (5:35:60)/Al_2O_3, Ru/Mn/Nd (5:30:65)/Al_2O_3, Ru/Mn/Nd (5:25:70)/Al_2O_3, Ru/Mn/Nd (5:20:75)/Al_2O_3 and Ru/Mn/Nd (5:15:80)/Al_2O_3 calcined at 400 °C were 20%, 28%, 36%, 39%, 45% and 32% at 400 °C reaction temperatures, respectively. From the earlier screening, it was observed that Ru/Mn/Nd (5:20:75)/Al_2O_3 showed a promising catalytic activity among other catalysts. Therefore, this potential catalyst has been further investigated with various calcination temperatures.

Fig. 2 shows the effect of calcination temperature of Ru/Mn/Nd (5:20:75)/Al_2O_3 catalyst on CO_2 conversion. It can be seen that the CO_2 conversion reached 100% at 400 °C reaction temperature using a catalyst that was calcined at 1000 °C. Higher calcination temperature was more promising due to good dispersion of Nd_2O_3 on the catalyst surface. This is in good agreement with Duhan and Aghamkar who have concluded that calcination above 900 °C would activate the active species present on the catalyst surface [28]. Therefore, increasing calcination temperature would increase the catalytic activity in methanation reaction.

Ru/Mn/Nd (5:20:75)/Al_2O_3 catalyst containing different Nd based ratios were investigated to obtain the optimum based loading to enhance the catalytic activity. The CO_2 conversions at 400 °C reaction temperature are shown in Fig. 3, from which it can be seen that the catalytic performance was

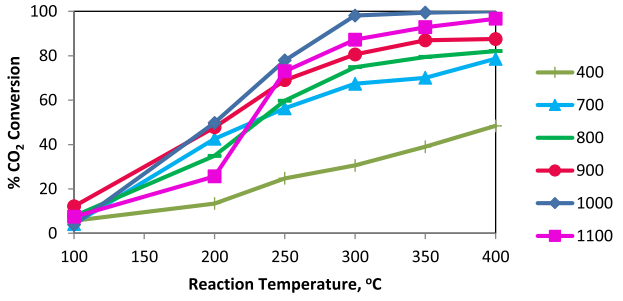

Fig. 2 Catalytic screening of Ru/Mn/Nd (5:20:75)/Al_2O_3 catalyst calcined at various calcination temperatures for 5 h.

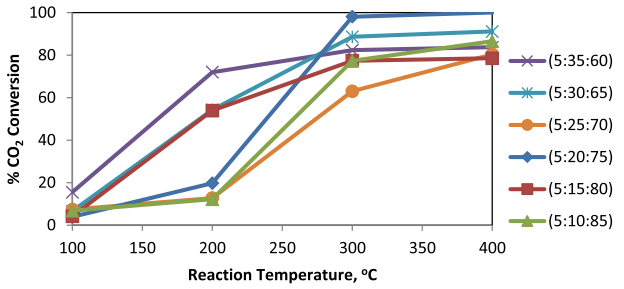

Fig. 3 Catalytic screening of Ru/Mn/Nd/Al_2O_3 catalyst calcined at 1000 °C with various metal oxides ratios at 400 °C reaction temperature.

obviously improved by the appropriate ratio of Nd based catalyst (75 wt%). The CO_2 conversion increased from 82% to 100% with the increase of Nd ratio from 60 wt% to 75 wt%, however, it declined to 84% as the Nd ratio increased to 85 wt%. The excessive amount of Nd might have blocked the active site as reported by He et al. [29] who found that the agglomeration of particle was occurred when increasing the amount of based catalyst resulting in the inhibition of the growth of the crystal which then blocked the surface active site. Perkas et al. [30] also stated that the lowest catalytic activity of catalyst was obtained when highest amount of based loadings was present and preventing the activation of the reagents.

The catalytic activity of Ru/Mn/Nd/Al_2O_3 catalyst was further explored by varying ruthenium loadings (5 wt%, 10 wt%, and 15 wt%). The CO_2 conversion of each catalyst started to drastically increase at 250 °C reaction temperature. In summary, the optimum ruthenium loadings to achieve higher CO_2 conversion was 5 wt% as the addition of small amount of noble metals could promote catalyst to achieve superior activity for methane formation [31]. This phenomenon was also in line with Zamani et al. [32] which reported that the addition of 5 wt% of ruthenium to based catalyst could enhance the catalytic activity by achieving almost 100% of CO_2 conversion. As shown in Fig. 4, it was observed that the incorporation of ruthenium into the manganese oxide catalyst showed a positive effect on the methanation reaction. This is similar to the finding by Panagiotopoulou et al. [33] where CO_2 methanation was strongly favored with the increasing of Ru content. Therefore, Ru/Mn/Nd (5:20:75)/Al_2O_3 catalyst was the best catalyst calcined at 1000 °C.

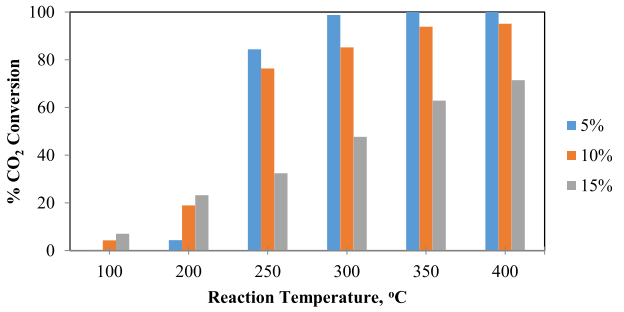

Fig. 4 CO_2 conversion of Ru/Mn/Nd (x:y:75)/Al_2O_3 catalyst calcined at 1000 °C for 5 h with various ruthenium loadings (x = 5%,10%,15%).

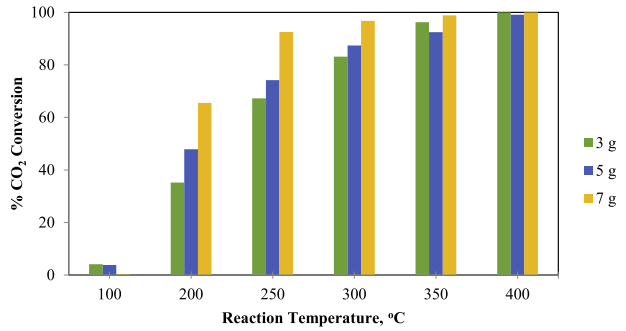

Fig. 5 CO_2 conversion of Ru/Mn/Nd (5:20:75) catalyst at various catalyst loadings calcined at 1000 °C for 5 h.

Optimization parameter with various loading of catalyst during reaction was also investigated as illustrated in Fig. 5. At reaction temperature of 200 °C, the CO_2 conversion started to increase drastically for each catalyst dosage. The highest CO_2 conversion was achieved with 7 g of catalyst dosage. This observation might be due to the increase in active site which was affected by the increase of catalyst loading. This finding was in a good agreement with Lu et al. [34] who found that the smaller amount of loading based exhibited a lower degradation rate due to inadequate catalytic active sites during the reaction.

3.2. Characterization

3.2.1. X-ray diffractogram (XRD) analysis

Diffractogram of Ru/Mn/Nd (5:20:75)/Al_2O_3 catalyst is shown in Fig. 6 by different calcination temperatures; 900 °C, 1000 °C and 1100 °C, respectively. The X-ray diffractograms pattern for all prepared catalysts exhibited polycrystalline peak. At calcination temperature of 900 °C, four peaks were observed and assigned to cubic Al_2O_3 which was emerged at 2θ of 39.42°, 45.79°, 60.54° and 66.85°. In addition, the peaks of RuO_2 with tetragonal phase were observed at 2θ of 28.10 and 36.53°, while Nd_2O_3 with cubic phase at 2θ of 28.61° and 33.21°. This result was in good agreement with Yadav et al. [35] who stated that Nd_2O_3 with cubic phase can only be seen when the catalyst was calcined at temperature more

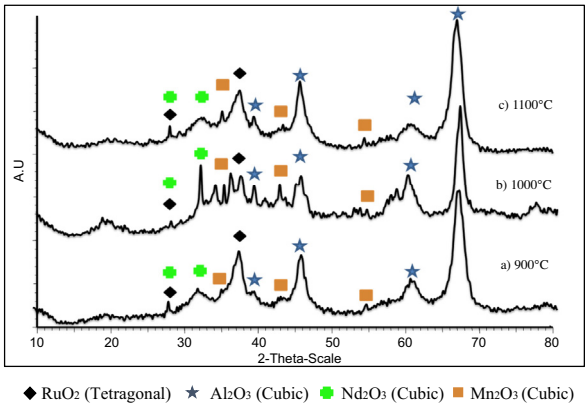

Fig. 6 XRD diffractogram of Ru/Mn/Nd (5:20:75)/Al_2O_3 catalyst calcined at various temperatures; 900 °C, 1000 °C and 1100 °C for 5 h.

than 200 °C. Another three small peaks observed at 34.83°, 42.90°, and 54.70° were corresponded to the cubic phase of Mn_2O_3. Similar species with the respected 2θ was observed for the diffractogram of 1000 °C calcination temperature. However, higher intensity for the Nd_2O_3 (2θ = 33.21°) and Mn_2O_3 (2θ = 34.83°, 42.90°) can be remarkably seen. The intensity of these peaks further decreased when increasing the calcination temperature up to 1100 °C. Therefore, it can be concluded that Mn_2O_3 and Nd_2O_3 species are the major active species that contribute to higher catalytic activity at 1000 °C calcination temperature.

3.2.2. Electron spin resonance (ESR)

ESR analysis was used to examine catalyst with unpaired spins which it interacts to each other, coherent electromagnetic radiation and the magnetic moments of neighboring nuclei [36]. The broad spectrum obtained was due to polycrystalline property of the catalyst resulted in wide distribution of the electron spin orientation [37] as the catalyst was in the polycrystalline structure as observed in XRD (Fig. 6). The g-value of 4.36 was attributed to the Al_2O_3 from the catalyst support while g-value of 2.35 exhibited "wing" on both sides was attributed to Nd^{3+} from Nd_2O_3 compound [38,39], as shown in Fig. 7. This result was reinforced with XRD analysis which showed the presence of Nd_2O_3 species. Comparing with XRD analysis, it can be observed that the peak of Nd_2O_3 was higher at 1000 °C, hence causing the increase in the amount of paramagnetic species which lead to the increment in its intensity as well as catalytic activity as compared to 900 °C and 1100 °C.

3.2.3. Temperature programmed reduction (TPR)

The H_2-TPR profile for Ru/Mn/Nd (5:20:75)/Al_2O_3 are shown in Fig. 8. At calcination temperature of 1000 °C, four

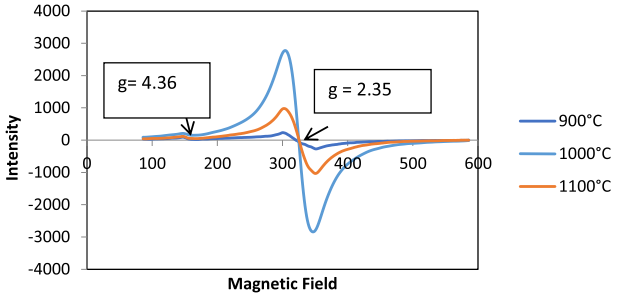

Fig. 7 ESR spectra of Ru/Mn/Nd (5:20:75)/Al_2O_3 catalyst calcined at (a) 900 °C, (b) 1000 °C, and (c) 1100 °C for 5 h.

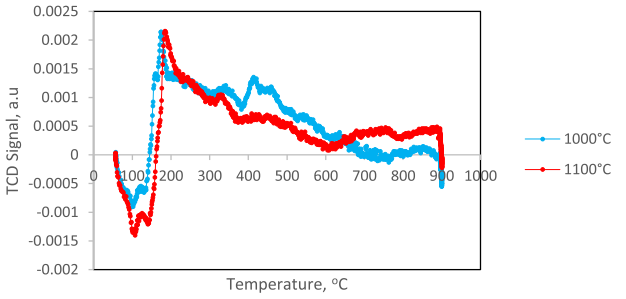

Fig. 8 H_2-TPR profile of Ru/Mn/Nd (5:20:75)/Al_2O_3 calcined at 1000 °C and 1100 °C for 5 h.

reduction peaks were observed at 189.9 °C, 461.4 °C, 724.5 °C and 879.2 °C. The first reduction peak at 189.9 °C was attributed to the reduction temperature for ruthenium species with total hydrogen consumption of 0.155 mmol/g STP. According to Li et al., a broad shoulder peak at 180–300 °C was attributed to the RuO_2 reduction to metal Ru [40] and this observation was also detected in XRD analysis. The second reduction peak at 461.4 °C with H_2 consumption of 0.09 mmol/g at STP was assigned to the reduction of Mn^{4+} to Mn^{2+} species which was in agreement with Peluso et al. [41]. Meanwhile, the third reduction peak (724.5 °C) was ascribed to the surface reduction of mixed metal oxides with total H_2 consumption was 0.018 mmol/g STP [42]. Meanwhile, 879.2 °C was assigned as the reduction of bulk oxygen of Nd_2O_3 with H_2 consumption was 0.018 mmol/g STP. Introduction of Nd^{3+} cation into the catalyst improves the mobility of oxygen into the lattice [42], therefore it contributed to higher catalytic activity at this calcination temperature. For calcination temperature of 1100 °C, all the reduction peaks observed showed a similar trend as those at 1000 °C. Peak shift occurs at higher temperatures up to 1100 °C due to strong interactions between metal oxides and carriers, therefore higher temperatures needed by active species to be reduced [43]. From the TPR profile, no reduction peak of γ-Al_2O_3 was observed, proving that γ-Al_2O_3 is an inert support.

3.2.4. CO_2-temperature programmed desorption (CO_2-TPD)

The CO_2-TPD profile of Ru/Mn/Nd (5:20:75)/Al_2O_3 revealed one desorption peaks at 148.2 °C with 1.56 mmol/g STP as shown in Fig. 9. It indicated that the peak was assigned to CO_2 adsorbed on the manganese species. The lowest desorption temperature was due to desorption of the weakest bonding mode of CO_2 onto a weak basic site on catalyst surface [42,44]. Consequently, it increased the catalytic activity of the catalyst at 1000 °C calcination temperature. Peak area at a lower temperature of 148.2 °C indicated that the chance for methane formation was higher.

3.2.5. Nitrogen adsorption (NA) analysis

The adsorption–desorption curve of Ru/Mn/Nd (5:20:75)/Al_2O_3 catalyst is depicted in Fig. 10. From the graph, the hysteresis formed around above 0.5P/Po suggested the type IV isotherm and H_3 hysteresis loop which is characteristic of solids consisting of non-rigid aggregates of plate-like particles forming a non-uniform slit-shaped pores [45,46]. The formations of the non-uniform channel within the pores would change the adsorption and desorption of the catalysts as well as increase the adsorption of active reactant [47]. The plot corresponds to the existence of mesopores and extension to the porous bottleneck form since monolayer was completed and the multilayer adsorption started to occur at high P/Po [18,48]. The obtained BET surface area at 900 °C, 1000 °C, and 1100 °C were 56.32 m^2/g, 83.67 m^2/g and 73.91 m^2/g with average pore diameter of 71.31 Å, 95.97 Å, and 72.13 Å respectively. These results suggested that 1000 °C is the most potential catalyst due to the higher surface area and average pore diameter which determine the higher catalytic activity as it gave space for the CO_2/H_2 to react on the surface of the catalyst.

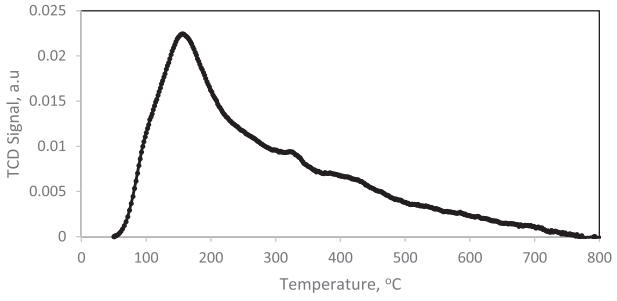

Fig. 9 CO_2-TPD curve of Ru/Mn/Nd (5:20:75)/Al_2O_3 calcined at 1000 °C for 5 h.

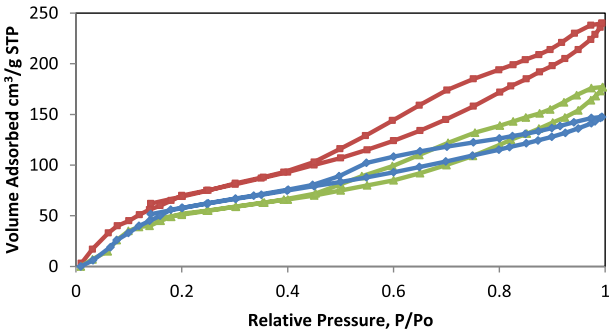

Fig. 10 Isotherm plots of Ru/Mn/Nd (5:20:75)/Al_2O_3 catalyst calcined at (a) 900 °C (♦), (b) 1000 °C (■), and (c) 1100 °C (▲) for 5 h.

3.2.6. Field emission scanning electron microscopy (FESEM)-Electron dispersion X-ray (EDX) analysis

The micrographs for Ru/Mn/Nd (5:20:75)/Al_2O_3 catalysts with calcination temperatures of 900 °C, 1000 °C, and 1100 °C are shown in Fig. 11. The micrographs showed an agglomeration of particles which are not homogenously affected by calcination temperature [49]. Some particles formed a flat slab which might attribute to the existence of Nd_2O_3 [44,50] and supported by XRD which showed the presence of this species on the catalyst surface. At 1000 °C calcination temperature, the particles seemed to be shattered and coalesce forming a larger particle and this event is consistent with previously reported literature [51], whereby addition of neodymium has led to shattered particle. This was possibly due to the porosity of alumina and oxygen vacancy of neodymium which caused the charging effects. The particle size of Ru/Mn/Nd (5:20:75)/Al_2O_3 catalysts calcined at 900 °C, 1000 °C, and 1100 °C is 108 nm, 123 nm, and 117 nm respectively. This particle size is larger due to lower surface area obtained from BET analysis as it form agglomeration particle.

EDX analysis gives information on the percentage of the elements existing on the sample surface, and the composition of the catalyst that was successfully coated on the support. From the Table 2, Mn was found to be higher percentage atomic ratio which might due to the higher affinity of Mn to be adsorbed on the surface. At 1000 °C calcination temperature, the atomic ratio for Nd, Ru and Mn was quite higher with 3.92%, 1.84% and 4.72%, respectively on the catalyst surface which contributed to higher activity at this temperature. This finding was supported with XRD analysis which showed a higher intensity of peak at 1000 °C compared to

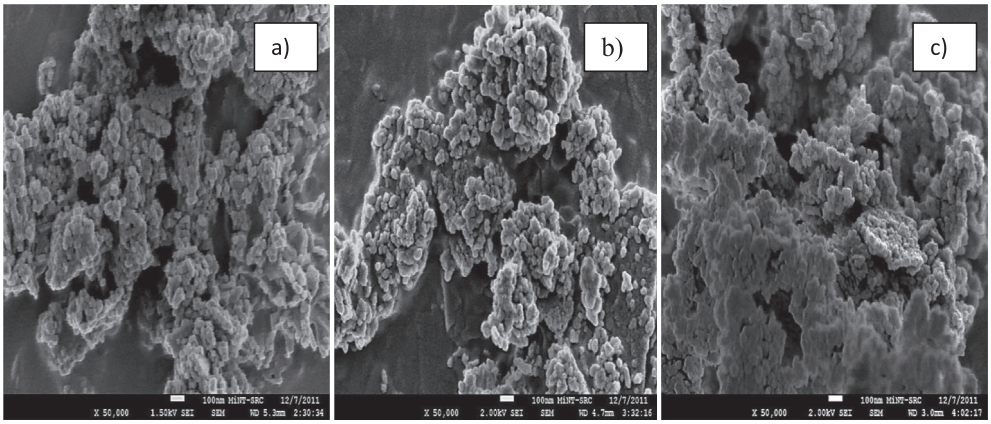

Fig. 11 FESEM micrographs of Ru/Mn/Nd (5:20:75)/Al_2O_3 catalyst calcined at (a) 900 °C, (b) 1000 °C, and (c) 1100 °C for 5 h in 50,000× magnification.

Table 2 EDX analysis for Ru/Mn/Nd (5:20:75)/Al_2O_3 catalysts calcined at 900 °C, 1000 °C, and 1100 °C for 5 h.

Calcination temperature, °C	Atomic ratio (%)				
	Al	O	Nd	Mn	Ru
900	32.32	46.10	2.44	4.48	0.46
1000	36.53	48.35	3.92	4.72	1.84
1100	31.50	51.54	3.15	4.64	0.70

other calcination temperature. All the active species were observed in XRD analysis.

3.2.7. Thermogravimetric analysis (TGA-DTA)

The evolution of weight loss with drying or decomposition of the dried catalyst is important to determine the maximum temperature after the catalyst is completely decomposed. This analysis also serves to establish the lowest temperature at which the catalyst is thermally stable and the lowest temperature for the calcination process. Fig. 12 shows a TGA-DTA thermogram obtained for Ru/Mn/Nd (5:20:75)/Al_2O_3 catalyst and the summarized results of TGA-DTA is tabulated in Table 3.

The first region of weight loss in the thermogram from 60 °C to 240 °C was attributed to the removal of bulk and physisorbed water. The first intense endothermic peak at DTA curve corresponded to the thermal desorption of water [52]. A broad endothermic peak appeared at 240–440 °C from

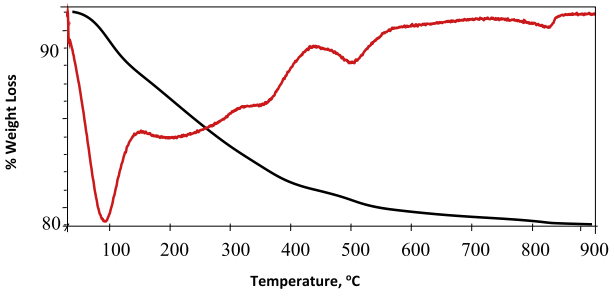

Fig. 12 TGA-DTA thermograms of as-synthesize of Ru/Mn/Nd (5:20:75)/Al_2O_3 catalyst.

Table 3 Summary results of TGA analysis of Ru/Mn/Nd (5:20:75)/Al_2O_3 catalyst.

Catalyst	Temperature (°C)	Weight loss (%)	Deduction
As-synthesize Ru/Mn/Nd (5:20:75)/Al_2O_3	60–240	10.60	Evaporation and elimination of the bulk and physisorbed water
	240–440	6.78	Decomposition of nitrate compound
	440–650	2.38	Loss of surface hydroxyl molecule
	650–900	0.90	Formation of phase-pure doped oxide

DTA curve, indicating the decomposition of nitrate ion that was entrapped in the pores of the support [53]. The peak at 320–440 °C was attributed to the abstraction of chemically bound water from aluminium hydroxide or the removal of structural water from the alumina [52]. The mass loss from 440 °C to 650 °C was attributed to the loss of surface hydroxyl molecule. The DTA curve showed an endothermic peak at around 520 °C which indicates the decomposition of water from the catalyst [54]. The presence of water molecule was due to the amorphous surface of the catalyst that was still covered with water and the hydrophilic nature of alumina. At 650–900 °C, an endothermic peak was observed at 860 °C in the DTA curve, indicating that the catalyst had undergone morphological and structural modifications which can be attributed to the formation of phase-pure doped oxide as reported by Ketzial et al. [55]. It could be concluded that pure metal oxide may have been formed after 900 °C, thus suggesting that calcination temperature of above 900 °C is adequate and capable of stabilizing the respective catalyst.

3.3. Methane formation using GC analysis

The potential Ru/Mn/Nd (5:20:75)/Al_2O_3 catalyst has been further investigated for methane formation using GC analysis. At room temperature, no CH_4 formation was observed as shown in Fig. 13 and tabulated in Table 4. Nonetheless, the

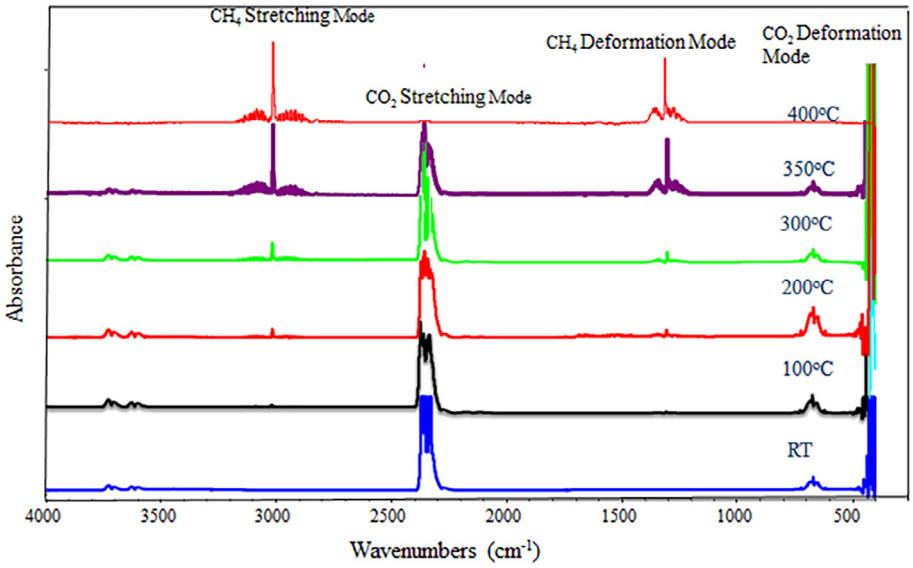

Fig. 13 Representative of the FTIR spectra showing CO_2 and CH_4 peaks which appeared during the CO_2/H_2 methanation reaction of Ru/Mn/Nd (5:20:75)/Al_2O_3 catalyst calcined at 1000 °C for 5 h.

Table 4 Testing results of in-situ reactions of methane formation over Ru/Mn/Nd (5:20:75)-Al_2O_3 catalyst at 1000 °C calcination temperature.

Catalyst	Reaction temperature (°C)	Converted CO_2 (%)*		Unreacted CO_2 (%)
		% Formation of CH_4	Formation of H_2O	
Ru/Mn/Nd (5:20:75)-Al_2O_3	RT	–	–	100.00
	100	1.29	5.29	93.42
	200	4.91	18.87	76.22
	300	10.00	58.66	31.34
	350	22.06	57.90	20.04
	400	40.32	59.68	–

* Calculation based on CO_2 detected via FTIR and CH_4 detected via GC.

percentage of CH_4 formation increased when increasing the reaction temperature up to 400 °C [56,57]. During reaction temperature at 100 °C, the catalytic CO_2 conversion could be due to the partial oxidation reaction since that the amount of unreacted CO_2 was higher than the formation of CH_4. Yaccato et al. [58] has investigated the formation of carbon monoxide as the main product at low temperature. However, in this study no CO formed at low reaction temperature due to no peak of CO observed on the FTIR spectrum (Fig. 13). It showed that CO_2 peak was more profound at the lower activation temperature of 300 °C. When the reaction temperature increased, the CO_2 peak was gradually diminished until almost CO_2 peaks disappeared at the catalytic reaction temperature of 400 °C. The percentage of CH_4 formation at 400 °C reaction temperature was 40.32% and the by-product formed was only water molecule [17,18].

4. Conclusion

The Ru/Mn/Nd/Al_2O_3 catalyst was highly active in methanation reaction. Almost 100% CO_2 conversion and over 40% CH_4 formation were achieved on Ru/Mn/Nd (5:20:75)/Al_2O_3 catalyst (calcination temperature was 1000 °C) at 400 °C reaction temperature under the condition of GHSV = 636 h^{-1}. XRD results indicated that the polycrystalline peaks in the spectrum with Nd_2O_3 and MnO_2 as an active species. These species were reduced over 400 °C which represented high basicity to the catalyst as observed in TPR and TPD analyses. This potential catalyst illustrated some agglomeration and undefined shape in FESEM analysis. ESR analysis showed paramagnetic properties of Nd_2O_3 species at 1000 °C which enhance higher catalytic activity. Ru/Mn/Nd (5:20:75)/Al_2O_3 catalyst calcined at 1000 °C could be regenerated under oxidation reaction and can be stabilized for 5 h with above 90% CO_2 conversion before deteriorated after 6 h.

Acknowledgement

The authors thank to Universiti Sultan Zainal Abidin, Universiti Teknologi Malaysia and Ministry of Higher Education (MOHE), Malaysia for financial support under FRGS, Vot 4F740.

Declaration of interest

The authors report no declarations of interest.

References

[1] R.N. Curry, Fundamental of natural gas conditioning, in: Technology & Engineering, PennWell Books Publishing Company, Oklahoma, 1981, pp. 66–67.

[2] C.W. Moore, B. Zielinska, G. Petron, R.B. Jackson, Air impacts of increased natural gas acquisition, processing, and use: a critical review, Environ. Sci. Technol. 48 (2014) 8349–8359.

[3] Pike Research, Forecast: 17M Natural Gas Vehicles Worldwide by 2015, Green Car Congress, 2009.

[4] A.A. Md. Yassin, Natural-gas future energy for Malaysia. Kuala Lumpur, Malaysia, Simposium Ketige Jurutera Kimia Malaysia, 1987.

[5] C. Shearer, J. Bistline, M. Inman, S.J. Davis, The effect of natural gas supply on US renewable energy and CO_2 emission, Environ. Res. Lett. 9 (2014) 094008.

[6] G.P. Zou, N. Cheranghi, F. Taheri, Fluid-induced vibration of composite natural gas pipelines, Int. J. Solids Struct. 42 (3–4) (2005) 1253–1268.

[7] A.Z. Ab Halim, R. Ali, W.A. Wan Abu Bakar, CO_2/H_2 methanation over M*/Mn/Fe-Al_2O_3 (M*: Pd, Rh, and Ru) catalysts in natural gas; optimization by response surface methodology-central composite design, Clean Technol. Environ. Policy 17 (3) (2015) 627–636.

[8] S.J.M. Rosid, W.A.W.A. Bakar, R. Ali, Physicochemical study of supported cobalt–lanthanum oxide-based catalysts for CO_2/H_2 methanation reaction, Clean Technol. Environ. Policy 17 (1) (2015) 257–264.

[9] A.H. Zamani, R. Ali, W.A.W. Abu Bakar, Optimization of CO_2 methanation reaction over M*/Mn/Cu-Al_2O_3 (M*: Pd, Rh, and Ru) catalysts, J. Ind. Eng. Chem. 29 (2015) 238–248.

[10] B.V. Ayodele, S.S. Hossain, S.S. Lam, O.U. Osazuwa, M.R. Khan, C.K. Cheng, Syngas production from CO_2 reforming of methane over neodymium sesquioxide supported cobalt catalyst, J. Nat. Gas Sci. Eng. 34 (2016) 873–885.

[11] H.V. Fajardo, E. Longo, L.F.D. Probst, A. Valentini, N.L.V. Carreno, M.R. Nunes, A.P. Maciel, E.R. Leite, Influence of rare earth doping on the structural and catalytic properties of nanostructured tin oxide, Nanoscale Res. Lett. 3 (5) (2008) 194–199.

[12] S. Sato, R. Takahashi, M. Kobune, H. Gotoh, Basic properties of rare earth oxides, Appl. Catal. A Gen. 356 (1) (2009) 57–63.

[13] S.G. Wang, X.Y. Liao, D.B. Cao, C.F. Huo, Y.W. Li, J.G. Wang, H.J. Jiao, Factors controlling the interaction of CO_2 with transition metal surfaces, J. Phys. Chem. C 111 (45) (2007) 16934–16940.

[14] N.A. Buang, W.A.W. Abu Bakar, W.M.Y. Othman, Studies on Supported Rare Earth Metal Catalyst with High Specific Activity and Selectivity towards Carbon Dioxide Removal in Natural Gas via Methanation Reactor, Report Thesis, Universiti Teknologi Malaysia, Skudai, 2005.

[15] S. Toemen, W.A.W. Abu Bakar, R. Ali, Investigation of Ru/Mn/Ce/Al_2O_3 catalyst for carbon dioxide methanation: Catalytic optimization, physicochemical studies and RSM, J. Taiwan Inst. Chem. Eng. 45 (2014) 2370–2378.

[16] S.J.M. Rosid, W.A.W.A. Bakar, R. Ali, Characterization and modelling optimization on methanation activity using Box-Behnken design through cerium doped catalysts, J. Clean. Prod. 170 (2018) 278–287.

[17] S.J.M. Rosid, W.A.W. Abu Bakar, R. Ali, Methanation reaction over samarium oxide based catalysts, Malaysian J. Fundamental Appl. Sci. 9 (1) (2013) 28–34.

[18] S.J.M. Rosid, W.A.W. Abu Bakar, R. Ali, Optimization of praseodymium oxide based catalysts for methanation reaction of simulated natural gas using Box-Behnken design, Jurnal Teknologi. 75 (1) (2015) 55–65.

[19] D. Wierzbicki, R. Debek, M. Motak, T. Grzybek, M.E. Galvez, P. Da costa, Novel Ni-La-hydrotalcite derived catalysts for CO_2 methanation, Catal Commun. 83 (2016) 5–8.

[20] K. Stangeland, D. Kalai, H. Li, Z. Yu, CO_2 methanation: the effect of catalysts and reaction conditions, Energy Procedia 105 (2017) 2022–2027.

[21] B. Roy, S. Chakrabarty, O. Mondal, M. Pal, A. Dutta, Effect of neodymium doping on structure, electrical and optical properties of nanocrystallite ZnO, Mater. Charact. 70 (2012) 1–7.

[22] M. Harilal, V.M. Nair, P.R.S. Wariar, K.P. Padmasree, M.M. Yusoff, R. Jose, Electrical and optical properties of $NdAlO_3$ synthesized by an optimized combustion process, Mater. Charact. 90 (2014) 7–12.

[23] R. Long, H. Wan, Promotion by strontium fluoride of neodymium oxide catalysis of the oxidative coupling of methane, J. Chem. Soc., Faraday Trans. 94 (8) (1998) 1129–1135.

[24] M.H. Razali, W.A.W. Abu Bakar, N.A. Buang, Global CO_2 recycling through methanation reaction using neodymium doped nickel oxide catalyst, J. Sustain. Sci. Manage. 5 (2) (2010) 148–152.

[25] Y. Zhu, S. Zhang, Y. Ye, X. Zhang, L. Wang, W. Zhu, F. Cheng, F. Tao, Catalytic conversion of carbon dioxide to methane on ruthenium-cobalt bimetallic nanocatalysts and correlation between surface chemistry of catalysts under reaction conditions and catalytic performances, ACS Catal. 2 (11) (2012) 2403–2408.

[26] J. Gao, C. Jia, J. Li, M. Zhang, F. Gu, G. Xu, Z. Zhong, F. Su, Ni/Al_2O_3 catalysts for CO methanation: Effect of Al_2O_3 supports calcined at different temperatures, J. Energy Chem. 22 (6) (2013) 919–927.

[27] P. Su, D. Chu, L. Wang, Studies on catalytic activity of nanostructure Mn_2O_3 prepared by solvent-thermal method on degrading crystal violet, Modern Appl. Sci. 4 (5) (2010) 125–129.

[28] S. Duhan, P. Aghamkar, Influence of temperature and time on Nd_2O_3-SiO_2 composite prepared by the sol-gel process, Acta Phys. Polonica A 113 (6) (2008) 1671–1672.

[29] L. Zhang, H.Q. He, H.G. Wu, C.H. Li, S.P. Jiang, Synthesis and characterization of doped $La_9ASi_{6026.5}$ (A = Ca, Sr, Ba) oxyapatite electrolyte by water-based gel-casting route, Int. J. Hydrogen Energy 36 (11) (2011) 6862–6874.

[30] N. Perkas, G. Amirian, Z. Zhong, J. Teo, Y. Gofer, A. Gedanken, Methanation of carbon dioxide on Ni catalysts on mesoporous ZrO_2 doped with rare earth Oxides, Catal. Lett. 130 (3–4) (2009) 455–462.

[31] S. Sharma, Z. Hu, P. Zhang, E.W. McFarland, H. Metiu, CO_2 methanation on Ru-doped Ceria, J. Catal. 278 (2) (2011) 297–309.

[32] A.H. Zamani, R. Ali, W.A. Wan, Abu Bakar. The investigation of Ru/Mn/Cu-Al_2O_3 oxide catalysts for CO_2/H_2 methanation in natural gas, J. Taiwan Instit. Chem. Eng. 45 (1) (2014) 143–152.

[33] P. Panagiotopoulou, D.I. Kondarides, X.E. Verykios, Selective methanation of CO over supported Ru catalysts, Appl Catal. B: Environ. 88 (3–4) (2009) 470–478.

[34] C.S. Lu, C.C. Chen, L.K. Huang, P.A. Tsai, H.F. Lai, Photocatalytic degradation of Acridine Orange over $NaBiO_3$ driven by visible light irridation, Catalysts 3 (2) (2013) 501–516.

[35] M.K. Yadav, B. Sanyal, A. Mookerjee, Stabilization of ferromagnetism in Mn doped ZnO with C Co-doping, J. Magn. Magn. Mater. 321 (4) (2009) 273–276.

[36] R. Stober, W. Herrmann, Isotope effects in ESR spectroscopy, Molecules 18 (6) (2013) 6679–6722.

[37] S. Maron, G. Dantelle, T. Gacoin, F. Devreux, NMR and ESR relaxation in Nd and Gd doped $LaPO_4$: towards the accurate determination of the doping concentration, PCCP 16 (35) (2014) 18788–18798.

[38] R. Jablonski, S.M. Kaczmarek, M. Swirkowicz, T. Lukasiewicz, Electron spin resonance and optical measurements of yttrium

ortho-vanadate doped with Nd^{3+} ions, J. Alloys Comp. 300-301 (2000) 310–315.
[39] S.I. Arockiam, A.P.P. Regis, L.J. Berchmans, Synthesis and characterisation of Nano crystalline Cerium nickelate ($CeNiO_3$) powders using low temperature molten salt technique, Int. J. ChemTech. Res. 4 (2) (2012) 798–804.
[40] T. Li, Y. Yang, C. Zhang, X. An, H. Wan, Z. Tao, H. Xiang, Y. Li, F. Yi, B. Xu, Effect of manganese on an iron-based Fischer-Tropsch synthesis catalyst prepared from ferrous sulfate, Fuel 86 (7–8) (2007) 921–928.
[41] M.A. Peluso, W.Y. Hernandez, M.I. Dominguez, H.J. Thomas, M.A. Centeno, J.E. Sambeth, CO oxidation: effect of Ce and Au addition on MnOx catalysts, Lat. Am. Appl. Res. 42 (4) (2012) 351–358.
[42] L.P.S. Xavier, V. Rico-Perez, A.M. Hernandez-Gimenez, D. Lozano-Castello, A. Bueno-Lopez, Simultaneous catalytic oxidation of carbon monoxide, hydrocarbons and soot with Ce-Zr-Nd mixed oxides simulated diesel exhaust conditions, Appl. Catal. B Environ. 162 (2015) 412–419.
[43] W.P. Dow, Y.P. Wang, T.J. Huang, TPR and XRD studies of yttria-doped ceria/γ-alumina supported copper oxide catalyst, Appl. Catal. A 190 (1–2) (2000) 25–34.
[44] Y. Zhang, G. Zhang, L. Wang, Y. Xu, Y. Sun, Selective methanation of carbon monoxide over Ru based catalysts in H_2-rich gases, J. Ind. Eng. Chem. 18 (5) (2012) 1590–1597.
[45] M. Thommes, K. Kaneko, A.V. Neimark, J.P. Olivier, F. Rodrigue-Reinoso, J. Rouquerol, K.S.W. Sing, Physisorption of gases, with special reference to the evaluation of surface area and pore size distribution (IUPAC Technical Report), Pure Appl. Chem. 87 (9–10) (2015) 1051–1069.
[46] K. Sing, The use of nitrogen adsorption for the characterisation of porous materials, Colloids Surfaces A: Physicochem. Eng. Aspects 187–188 (2001) 3–9.
[47] S.T. Hussain, R. Naheed, A. Badshah, T. Mohmood, Design and synthesis of nanoheterogeneous supported catalysts for olefin polymerization, African J. Pure Appl. Chem. 3 (12) (2009) 247–261.
[48] S. Lowell, J.E. Shields, M.A. Thomas, M. Thommes, Characterization of porous solids and powders: surface area, pore size, and density, Kluwer Academic Publishers, The Netherlands, 2004.
[49] R. Ali, W.A.W. Abu Bakar, N. Sulaiman, H.F. Abdul Rahim, Manganese oxide doped noble metals supported catalyst for carbon dioxide methanation reaction, Trans. C: Chem. Chem. Eng. Scientia Iranica 17 (2) (2010) 115–123.
[50] J.F. Read, The decomposition of Nitrous Oxide on Neodymium Oxide, Dysprosium Oxide and Erbium Oxide, J. Catal. 28 (3) (1973) 428–441.
[51] V. Anbarasu, A. Manigandan, K. Sivakumar, Structural, magnetic, and dielectric studies on strontium substituted Nd_2CuO_4 system, J. Modern Phys. 1 (2) (2010) 93–99.
[52] J. Guo, H. Lou, H. Zhao, D. Chai, X. Zheng, Dry reforming of methane over nickel catalyst supported on magnesium aluminate spinels, Appl. Catal. A: Gen. 273 (1–2) (2004) 75–82.
[53] P.G. Savva, K. Goundani, J. Vakros, K. Bourikas, C. Fountzoula, D. Vattis, A. Lycourgthiotis, C. Kordulis, Benzene hydrogenation over Ni/Al_2O_3 catalyst prepared by conventional and sol-gel techniques, Appl. Catal. B 79 (3) (2008) 199–207.
[54] P. Bera, M. Rajamathi, M.S. Hedge, P.V. Kamath, Thermal behaviour of hydroxides, hydroxysalt and hydrotalcites, Bull. Mater. Sci. 23 (2) (2000) 141–145.
[55] J.S.S.J. Ketzial, D. Radhika, A.S. Nesaraj, Low temperature preparation and physical characterization of doped $BaCeO_3$ nanoparticles by chemical precipitation, Int. J. Ind. Chem. 4 (18) (2013) 1–13.
[56] P. Djinovic, C. Galletti, S. Specchia, V. Specchia, CO methanation over $Ru-Al_2O_3$ catalysts: effect of chloride doping in reaction activity and selectivity, Top. Catal. 54 (2011) 1042–1053.
[57] S. Toemen, W.A.W. Abu Bakar, R. Ali, Effect of ceria and strontia over $Ru/Mn/Al_2O_3$ catalyst: Catalytic methanation, physicochemical and mechanistic studies, J. CO_2 Utiliz. 13 (2016) 38–49.
[58] K. Yaccato, R. Carhart, A. Hagemeyer, A. Lesik, P. Strasser, A. F. Volpe Jr, H. Turner, H. Weinberg, R.K. Grasselli, C. Brooks, Competitive CO and CO_2 Methanation over Supported noble metal Catalysts in High Throughput Scanning Mass Spectrometer, Appl. Catal. A 296 (1) (2005) 30–48.